


RESEARCH ARTICLE

Pseudophosphorylation of single residues of the J-domain of DNAJA2 regulates the holding/folding balance of the Hsc70 system

Lorea Velasco-Carneros^{1,2} | Ganeko Bernardo-Seisdedos^{3,4} |
Jean-Didier Maréchal⁵ | Oscar Millet³ | Fernando Moro^{1,2} | Arturo Muga^{1,2†} 

¹Instituto Biofisika (UPV/EHU, CSIC), University of Basque Country, Leioa, Spain

²Department of Biochemistry and Molecular Biology, Faculty of Science and Technology, University of the Basque Country (UPV/EHU), Leioa, Spain

³Precision Medicine and Metabolism Lab, CIC bioGUNE, Derio, Spain

⁴Department of Medicine, Faculty of Health Sciences, University of Deusto, Bilbao, Spain

⁵Insilichem, Departament de Química, Universitat Autònoma de Barcelona (UAB), Bellaterra (Barcelona), Spain

Correspondence

Arturo Muga and Fernando Moro, Instituto Biofisika (UPV/EHU, CSIC), Barrio Sarriena s/n, 48940 Leioa, Spain. Email: fernando.moro@ehu.eus

Funding information

Basque Government, Grant/Award Number: IT1745-22; MICIU/AEI/10.13039/501100011033, Grant/Award Number: PID2019-111068GB-I00; Viceconsejería de Universidades e Investigación

Review Editor: Aitziber L. Cortajarena

Abstract

The Hsp70 system is essential for maintaining protein homeostasis and comprises a central Hsp70 and two accessory proteins that belong to the J-domain protein (JDP) and nucleotide exchange factor families. Posttranslational modifications offer a means to tune the activity of the system. We explore how phosphorylation of specific residues of the J-domain of DNAJA2, a class A JDP, regulates Hsc70 activity using biochemical and structural approaches. Among these residues, we find that pseudophosphorylation of Y10 and S51 enhances the holding/folding balance of the Hsp70 system, reducing chaperone collaboration with Hsc70 while maintaining the holding capacity. Truly phosphorylated J domains corroborate phosphomimetic variant effects. Notably, distinct mechanisms underlie functional impacts of these DNAJA2 variants. Pseudophosphorylation of Y10 induces partial disordering of the J domain, whereas the S51E substitution weakens essential DNAJA2-Hsc70 interactions without a large structural reorganization of the protein. S51 phosphorylation might be class-specific, as all cytosolic class A human JDPs harbor a phosphorylatable residue at this position.

KEYWORDS

chaperone, DNAJA2, Hsc70, J-domain, phosphorylation, protein folding

† In memoriam.

1 | INTRODUCTION

The human genome encodes around 330 chaperones and cochaperones (Brehme et al., 2014; Hipp et al., 2019; Labbadia and Morimoto, 2015), among which 13 are Hsp70s, 50 J-domain proteins (JDs), and 14 nucleotide exchange factors (NEFs) (Rosenzweig et al., 2019). Although they can display specific functionalities, they usually work together to regulate protein folding, maintain the native conformation of proteins and direct unstable/misfolded proteins to degradation pathways (Jayaraj et al., 2020). An important player in all these functions is the Hsp70 system, which is composed of a central Hsp70 component and two accessory proteins that regulate the activity of the chaperone (Fernandez-Fernandez and Valpuesta, 2018; Rosenzweig et al., 2019). These accessory proteins are JDs and NEFs (Rosenzweig et al., 2019). JDs can display an autonomous, ATP-independent holding activity that avoids protein aggregation through their interaction with unstable, aggregation-prone conformations. They also select clients for Hsp70s and collaborate with the chaperone in ATP-dependent, substrate protein remodeling (Liu et al., 2020; Zhang et al., 2023). The large number of JDs, as compared with Hsp70s, suggests potential collaboration between different JDs and a particular Hsp70 in specific functions and relates expansion of the JDP family and functional diversification of the Hsp70 system. Hsp70s share a common structure with an N-terminal, nucleotide binding domain (NBD) with ATPase activity and a C-terminal substrate binding domain (SBD) interconnected by a flexible, conserved linker (Rosenzweig et al., 2019). In contrast, the JDP family is functionally and structurally diverse. This large degree of divergence seems to regulate substrate specificity, localization, ATPase, and substrate remodeling activities of Hsp70s (Craig and Marszalek, 2017; Kampinga and Craig, 2010; Zhang et al., 2023). Differences in protein length, domain organization, and function among members of the JDP family makes their classification challenging. They are usually grouped in three classes (A, B, and C) according to their domain organization. Classes A and B contain a characteristic J-domain (JD), after which the family was named, followed by a glycine/phenylalanine-rich region (G/FR), two C-terminal domains (CTDI and CTDII) that interact with the client protein, a dimerization domain (DD), and in some members a C-terminal domain (CD) (Velasco-Carneros et al., 2023). A unique structural feature in class A JDs is the insertion of a Zn-finger-like region in the CTDI (Figure 1a). Class C members contain a diversity of domains besides the JD (Zhang et al., 2023).

The J-domain of JDs folds into a similar hairpin structure with four helices (I–IV) (Figure 1b) and is responsible for their association with Hsp70. Despite this structural similarity, differences in the sequence within the structural

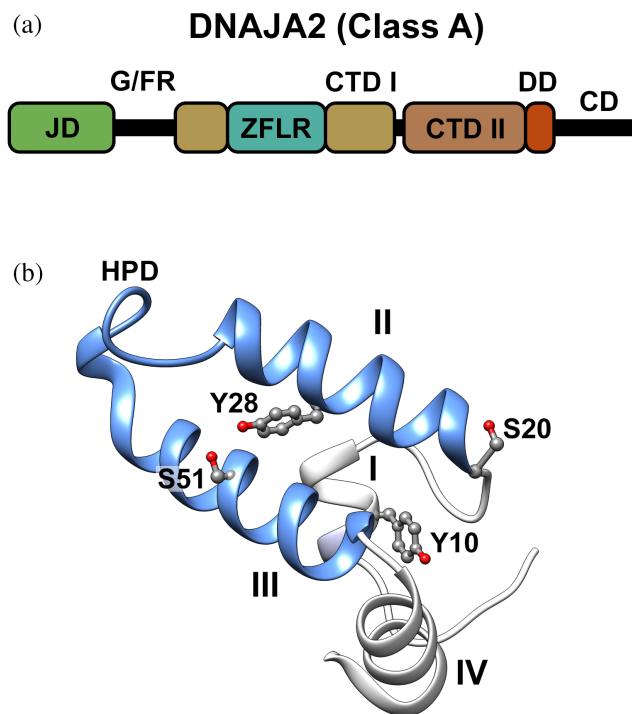


FIGURE 1 (a) Domain organization of DNAJA2. The scheme shows the J-domain (JD; green), the glycine/phenylalanine-rich region (G/FR), the two homologous β sandwich domains (CTDI and CTDII; khaki and brown), with a Zn²⁺ finger-like region (ZFLR; blue) inserted into the CTDI, the dimerization domain (DD; red), and the C-terminal domain (CD). (b) Predicted structure of DNAJA2 JD obtained by homology modeling. The tyrosine and serine residues replaced by glutamic acid in the phosphomimetic mutants are shown, and the interaction surface with Hsc70 (colored in blue the helix II, the connecting loop containing the HPD motif, and helix III) is colored in blue. CTD, C-terminal domain.

region that interacts with Hsp70 could regulate JDP-Hsp70 complex formation (Zhang et al., 2023). This region is formed by helices II and III and the loop containing the HDP motif that connects both helical segments (colored in blue in Figure 1b). A positively charged patch in helix II, close to the HDP motif, contacts a negatively charged one in the NBD of Hsc70, and helix III establishes hydrophobic interactions with the SBD of the chaperone, stabilizing the interaction with its interdomain linker (Ahmad et al., 2011; Kityk et al., 2018; Kleczewska et al., 2020; Malinverni et al., 2017). Domains other than the JD are involved in client selection, client transfer to Hsp70, intracellular location of JDP-Hsp70 complexes, and further modulate complex formation with the chaperone (Barriot et al., 2020; Dekker et al., 2015; Kampinga and Craig, 2010; Malinverni et al., 2023).

Despite the importance of the Hsp70 system in maintaining cell viability, our understanding on specific associations between members of the Hsp70 and JDP protein families linked to concrete functions, on the mechanisms of rewiring

the multiple Hsp70/JDP assemblies, and on how posttranslational modifications (PTMs) could regulate them remains limited. Proteomic approaches have revealed extensive PTMs in chaperones (Backe et al., 2020; Cloutier and Coulombe, 2013; Nitika et al., 2020; Omkar et al., 2023; Truman et al., 2021; Velasco et al., 2019), which most likely tune their activity. Despite the identification of these sites, the functional role of their modifications (collectively known as the Chaperone Code) are poorly understood and has been tested only for a few members of different chaperone families (Backe et al., 2020; Kostenko et al., 2014; Patel et al., 2016).

Here, we explore the effect that pseudophosphorylation of specific residues in the JD of class A JDPs (highlighted in Figure 1b) has on its interaction with substrate proteins and Hsc70. As scaffold, we use the JD of DNAJA2 that is considered one of the best suppressors of tau aggregation (Mok et al., 2018), and as the major cytosolic class A JDP also collaborates with Hsc70 in the reactivation of unfolded or aggregated proteins (Nillegoda et al., 2015). Although the JD can be phosphorylated in many residues, especially under stress conditions (Hornbeck et al., 2015), the functional consequences of these PTMs are so far unknown. We find that pseudophosphorylation of Y10 induces partial disordering of the J domain and impairs the remodeling activity of the Hsc70 system. The S51E phosphomimetic substitution induces localized rearrangements in helix III that disrupts contacts with the SBD of Hsc70, abolishing the disaggregating and refolding activities of the Hsp70 system. Phosphorylation of the same residues in isolated JDs promote similar conformational and functional effects, reinforcing data obtained with the phosphomimetic, full-length protein variants. Alignment of class A and class B JDPs also suggests that phosphorylation of S51 could be a class-specific regulation signal, mainly affecting to cytosolic class A human JDPs.

2 | RESULTS

2.1 | Design and evaluation of DNAJA2 variants with phosphomimetic substitutions in the J-domain

Residues in the JD of at least one member of class A human JDPs, found phosphorylated in high-throughput (HTP) experiments involving different human tumor cells and mitotic HeLa cells among others (Kettenbach et al., 2011; Mertins et al., 2014; Tsai et al., 2015) and listed in PhosphoSitePlus repository (Hornbeck et al., 2015), were considered candidates to study. Thus, Y10, S20, Y28, and S51 were selected and replaced by glutamic acid (pseudophosphorylated mutants) or alanine (non-phosphorylatable variants) in the JD of DNAJA2, which was used as scaffold to evaluate the effect of the

phosphomimetic substitutions (Figure 1b). This experimental strategy encounters two limitations. First, the substitution of a phosphorylated residue with glutamic acid does not replicate the net charge alteration of the phosphoryl group (-1 and -2 for glutamate and phosphoryl group, respectively). Second, the use of glutamate to simulate tyrosine phosphorylation might modify protein structure due to the lack of the aromatic ring (Beebe et al., 2013; Stateva et al., 2015). This limitation warrants consideration when evaluating the impact of phosphomimetic substitutions of specific tyrosine residues located in the hydrophobic protein core, which could compromise its stability (Subramanyam et al., 2016). In particular, Y10 is located in a solvent-exposed protein region of helix I, whereas the aromatic moiety of Y28 participates in the hydrophobic core formed by the antiparallel amphipathic helices II and III (Figure 1b), which contribute to JD stability (Qian et al., 1996). Despite these limitations, this strategy has been effective to investigate the biological function of phosphorylation (Bachman et al., 2018; Muhlhofer et al., 2021; Perez-Mejias et al., 2020).

A preliminary assessment of these variants was based on their ability to assist Hsc70 in substrate remodeling (disaggregating/refolding and refolding activities) and to protect client proteins against aggregation (holding activity). Potential candidates underwent a subsequent filtering step that considered the functional outcome of their replacement by alanine. Three different behaviors were observed for the phosphomimetic substitutions of the four amino acids shown in Figure 1b. First, substitution of S20 induced a modest decrease in Hsc70 activation (10%–15%) and substrate remodeling (10%–20%) (Figure S1A,B in Data S1). A second one was detected for Y28, whose replacement by either E or A yielded an almost complete inhibition of Hsc70 activation and substrate remodeling activity (Figure S1A,B in Data S1), which makes difficult to attribute a regulatory function to Y28 pseudophosphorylation. As expected from the involvement of the JD in the interaction with Hsc70, phosphomimetic substitutions only affected the client remodeling activity, leaving the holding activity largely unaltered (Figure S1C in Data S1). Finally, the third one was noted for Y10 and S51, where the phosphomimetic substitution significantly reduced the refolding activity of the Hsc70 system, while the mutation to A had little or no effect. Only these residues were further characterized as follows.

2.2 | Pseudophosphorylation of Y10 and S51 regulates the activity of the Hsc70 system

We analyzed in detail the phosphomimetic mutants DNAJA2-Y10E and DNAJA2-S51E, as well as the

corresponding non-phosphorylatable substitutions (Guo et al., 2015; Kao et al., 2020; Morishima et al., 2018), DNAJA2-Y10A and DNAJA2-S51A.

2.2.1 | Pseudophosphorylation of Y10 impairs assistance of Hsc70 during client remodeling

Y10 is located in helix I of the JD (Figure 1b), on the face opposite to the interacting surface with Hsc70 (Tomiczek et al., 2020). Both, Y10A and Y10E variants of DNAJA2 lost around 14% of the wt ability to stimulate Hsc70 ATPase activity (Figure 2a). It is important to note that the intrinsic ATPase activity of Apg2 ($0.7 \mu\text{mol ATP}/\text{min} \times \mu\text{M Apg2}$)

was not affected by DNAJA2 ($0\text{--}5 \mu\text{M}$), and thus only Hsc70 was activated by the JDP in the ternary mixture. A notable difference between both variants emerged when evaluating their cooperation with Hsc70 in aggregate reactivation (disaggregating/refolding activity). The activity of the non-phosphorylatable and the phosphomimetic mutants decreased 35% and 70%, respectively (Figure 2b), when compared to the wt protein. Similar differences between the Y10 variants were observed for their folding activity (Figure 2c). In this case, the client—luciferase—was chemically unfolded and diluted in the presence of wt DNAJA2 or the corresponding Y10 mutant to prevent its aggregation. Subsequently, Hsc70 and Apg2, the other two components of the chaperone system, and ATP were added to refold the DNAJA2-bound, unfolded substrate. DNAJA2-Y10A

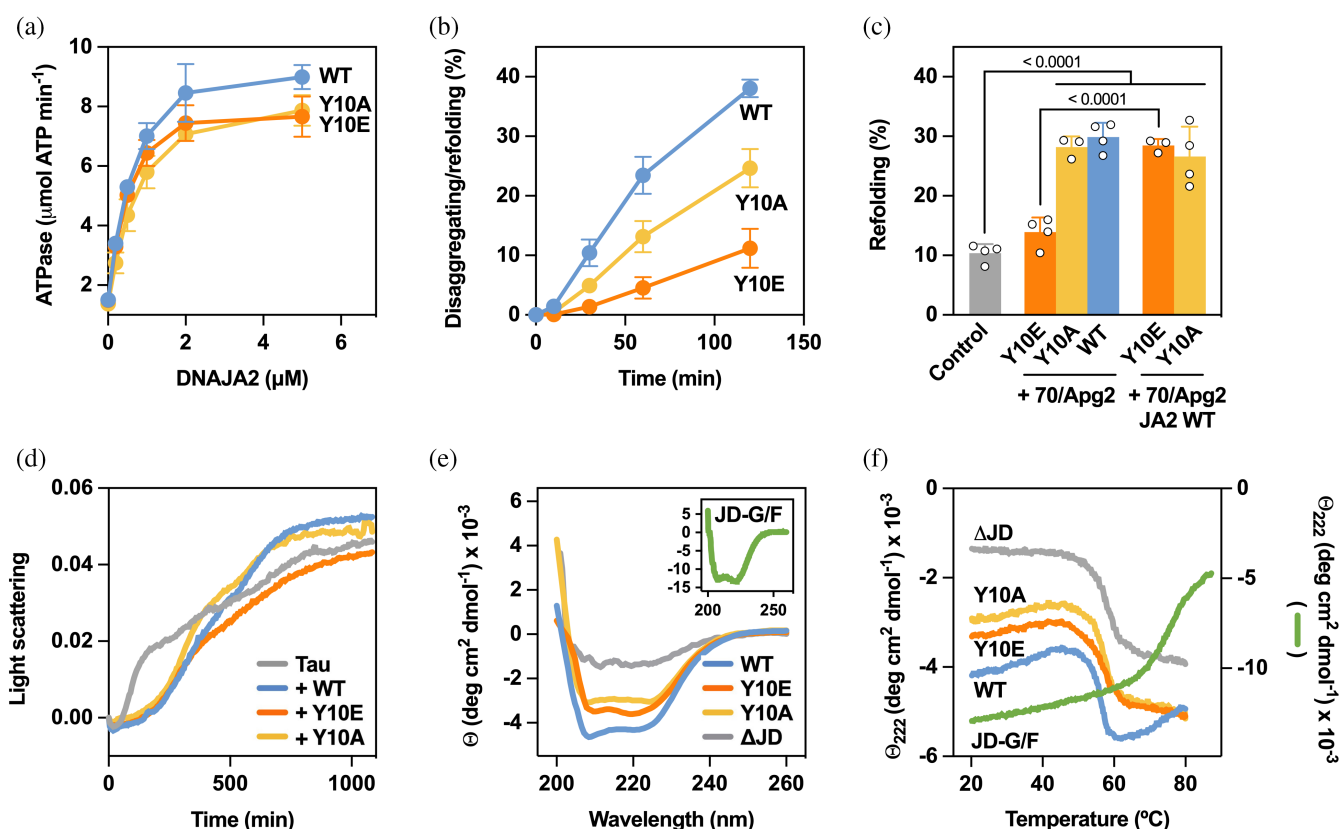


FIGURE 2 Functional and conformational properties of the single point mutants DNAJA2-Y10E and DNAJA2-Y10A. (a) Stimulation of the ATPase activity of Hsc70 ($2 \mu\text{M}$) in samples containing $0.4 \mu\text{M}$ Apg2, 2mM ATP, and increasing concentrations of wt DNAJA2 (blue), DNAJA2-Y10E (orange), or DNAJA2-Y10A (yellow). The same color code is used in all panels. (b) Reactivation of luciferase aggregates (20 nM) obtained at 42°C by $2 \mu\text{M}$ Hsc70, $0.4 \mu\text{M}$ Apg2, 2mM ATP, and $0.5 \mu\text{M}$ JDP. (c) Refolding activity of the different DNAJA2 species in collaboration with Hsc70. Luciferase ($10 \mu\text{M}$) was denatured in 6M urea and diluted 100 times in the absence (control, gray) or presence of $1 \mu\text{M}$ wt DNAJA2, DNAJA2-Y10E, or DNAJA2-Y10A. Afterwards, $2 \mu\text{M}$ Hsc70, 2mM ATP, and $0.4 \mu\text{M}$ Apg2 were added to the samples and luciferase recovery was measured after 120 min. To dissect the holding and refolding activities of the protein variants, they were also supplied with $1 \mu\text{M}$ DNAJA2 (right columns). (d) Effect of the different DNAJA2 species on the aggregation of Tau K18 P301L. Light scattered by samples containing equimolar amounts ($20 \mu\text{M}$) of tau and heparin in the absence (gray) and presence of $6 \mu\text{M}$ wt DNAJA2 or its Y10 variants. (e) Far-UV CD spectra of wt DNAJA2 and its Y10 mutants recorded at 25°C . Data corresponding to a DNAJA2 mutant that lacks the JD, DNAJA2 ΔJ (gray), and to a construct that contains the JD and G/FR (green; inset) are also shown. (f) Thermal stability of the same samples shown in (e) followed by the temperature dependence of the ellipticity at 222 nm . Values in panels (a)–(c) are means \pm s.d. of at least three independent experiments. CD, circular dichroism; JD, J-domain.

behaved akin to the wt protein, but the phosphomimetic mutation Y10E resulted in a two-fold reduction of the folding activity, which approached values similar to those obtained when dilution proceeded in the absence of chaperones (Figure 2c, control). To test if the refolding activity decrease could stem from an impaired interaction between the Y10E mutant and the denatured client, we added wt DNAJA2 together with Hsc70 and Apg2 in the refolding step, obtaining a recovery yield similar to that observed for the wild-type protein (Figure 2c; right columns). This finding suggests that both the Y10A and Y10E DNAJA2 variants display a wt-like holding activity; otherwise, the refolding extent would be similar to that observed in the control experiment. This was also demonstrated using a fragment of Tau containing the region responsible for protein aggregation (Figure 2d), whose onset of aggregation was delayed similarly by wt DNAJA2 and its Y10 variants.

A plausible explanation for the observed defective interaction of the phosphomimetic variant with Hsc70 could be that a conformational rearrangement of the JD upon Y10 substitution impaired assistance of Hsc70 during substrate remodeling. This hypothesis was tested by analyzing the secondary structure and thermal stability of the two DNAJA2 mutants by circular dichroism (CD) (Figure 2e). Data showed that substitution of Y10 by either E or A induced a conformational rearrangement evidenced by a reduction in the ellipticity value at 222 nm, compatible with a partial loss of helical content. This structural change was also seen by the disappearance of the thermal transition observed for the wt protein above 60°C, which was assigned to JD denaturation using a JD deletion mutant of DNAJA2 (DNAJA2 Δ JD) and a construct that contains the JD and the G/F region (JD-G/FR) (Figure 2e,f). Therefore, Y10 is most likely engaged in the stabilization of the JD as both substitutions induced a partial loss of the helical structure and the disappearance of the cooperative JD unfolding event. Although this partially unfolded conformation is able to stimulate Hsc70, it does not properly assist the chaperone in substrate remodeling. The distinctive functional outcome of the E and A replacements points to the negative charge at this position as a factor that regulates assistance to Hsc70 during client remodeling.

2.2.2 | Phosphorylation of S51 could function as a reversible switch that controls the interaction of DNAJA2 with Hsc70

As done with Y10, we analyzed the single point mutants DNAJA2-S51E and DNAJA2-S51A. In contrast to Y10,

none of the S51 mutants induced significant changes in the far-UV CD spectra and shape of the thermal unfolding curves (Figure S2 in Data S1). The first difference between these mutants was related to their ability to stimulate Hsc70 ATPase activity (Figure 3a). While DNAJA2-S51A showed a wt-like behavior, DNAJA2-S51E was around 85% less effective than wt DNAJA2 (Figure 3a). Next, we analyzed the collaboration of these mutants with Hsc70 in the reactivation of luciferase aggregates. DNAJA2-S51A behaved as the wt protein, whereas the disaggregating/refolding activity of DNAJA2-S51E was markedly diminished, reaching only 10% of the value observed for wt DNAJA2 (Figure 3b, left panel). This would be expected if JDP-mediated coordination of substrate binding and ATP hydrolysis in Hsc70, which is essential to extract unfolded monomers from the aggregate for their subsequent refolding (Cabrera et al., 2019; Kirstein et al., 2017), is compromised. To prove it, we first demonstrated that the difference in the disaggregating/refolding activity between the S51 variants was also observed using aggregates of glucose-6-phosphate dehydrogenase (G6PDH), indicating that it was substrate-independent (Figure 3b, right panel). Then, the ability of wt DNAJA2 and its two protein variants to interact with G6PDH aggregates, and to recruit Hsc70 was analyzed in the presence of Apg2, which favors chaperone transfer to the aggregate surface (Cabrera et al., 2022). Both DNAJA2 variants interacted with G6PDH aggregates similarly to the wt protein, but DNAJA2-S51E recruited two-fold less Hsc70 than wt DNAJA2 (Figure 3c,d). Therefore, the impaired disaggregating/refolding activity of this mutant is most likely due to its deficient chaperone recruitment at the aggregate surface.

The same interpretation could explain the folding activity, for example, the recovery of non-aggregated, cochaperone-bound unfolded clients, of these variants. DNAJA2-S51E, but not DNAJA2-S51A, displayed a strongly diminished Hsc70-dependent refolding activity (Figure 3e). To test whether DNAJA2-S51E protected luciferase from aggregation, that is, retained its holding activity despite being unable to assist Hsc70 in client refolding, we supplemented the sample with wt DNAJA2. Under these conditions, the refolding activity became wt-like (Figure 3e; right columns), indicating that the phosphomimetic mutant binds unfolded luciferase as the non-phosphorylatable variant and the wt protein. This suggestion was further supported by the wt-like ability of both S51 mutants to delay tau aggregation (Figure 3f). Taken together, these data indicate that the three protein species interact similarly with unfolded or aggregated clients, but DNAJA2-S51E is unable to collaborate with Hsc70 in client remodeling.

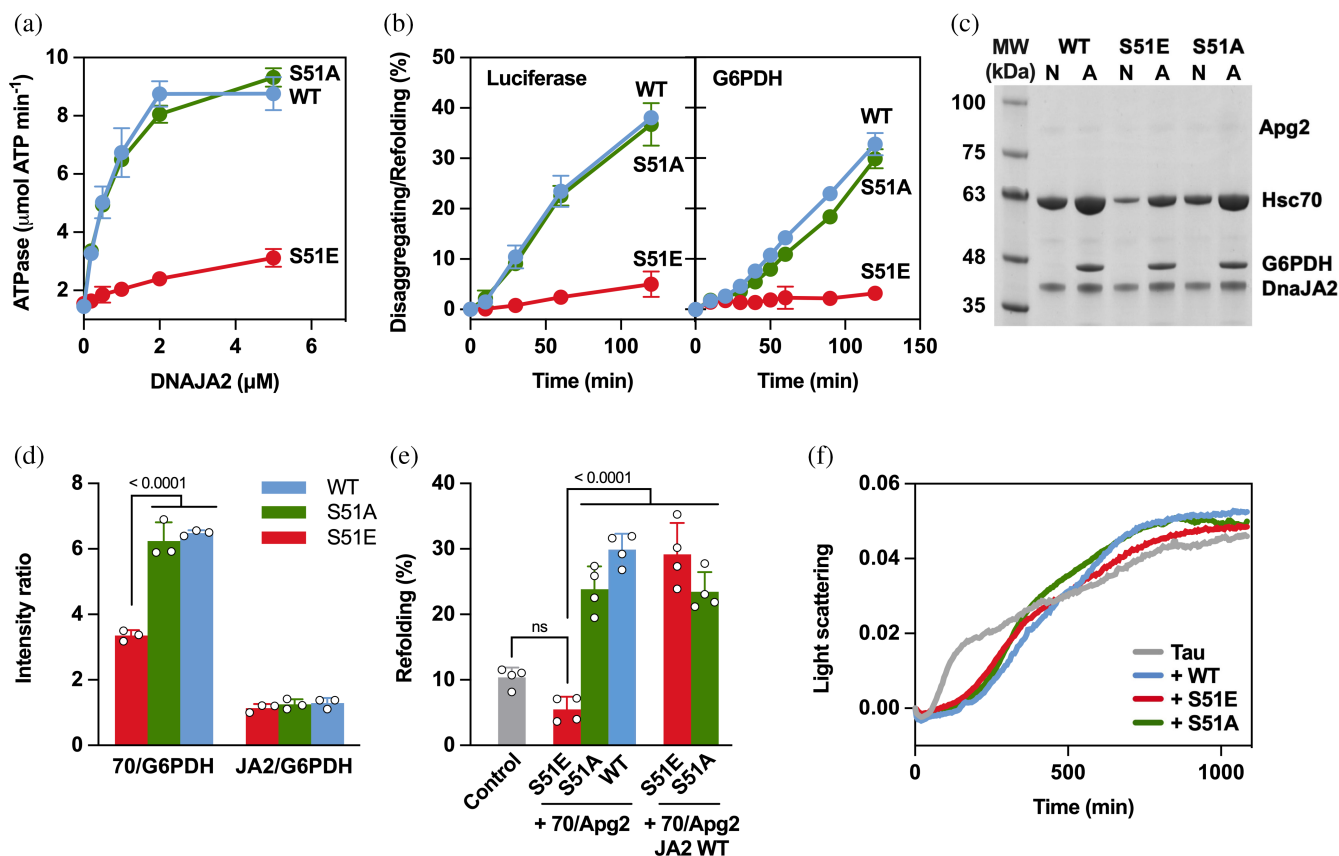


FIGURE 3 Pseudophosphorylation of S51 hinders productive interaction of DNAJA2 with Hsc70. (a) Stimulation of the ATPase activity of 2 μM Hsc70 by increasing concentrations of wt DNAJA2 (blue), DNAJA2-S51E (red), or DNAJA2-S51A (green) in the presence of 0.4 μM Apg2 ($n = 3$). Color code in all panels as in (a). (b) Recovery of 20 nM luciferase (left panel) and 0.4 μM G6PDH (right panel) aggregates after reactivation with 0.5 μM wt DNAJA2, DNAJA2-S51E, or DNAJA2-S51A, 2 μM Hsc70 and 2 mM ATP in the presence of 0.4 μM Apg2. (c) Interaction of the different DNAJA2 species and Hsc70 with native (N) or aggregated (A) G6PDH. (d) Binding of the different DNAJA2 species (JA2/G6PDH intensity ratio), and JDP-dependent Hsc70 recruitment (70/G6PDH intensity ratio) to the aggregate surface. Data from gels as that shown in (c). (e) Luciferase refolding by the different DNAJA2 species in collaboration with Hsc70. Luciferase (10 μM) denatured in 6 M urea was diluted 100 times in the absence (gray) or presence of 1 μM DNAJA2 or the corresponding S51 variant. Samples were supplied with 2 μM Hsc70, 2 mM ATP, and 0.4 μM Apg2, and luciferase recovery was measured after 120 min. Additionally, wt DNAJA2 was added to the samples containing the S51 mutants to distinguish their holding and refolding activities (right columns). (f) The three DNAJA2 species protect similarly against Tau aggregation. Light scattering of samples containing equimolar amounts (20 μM) of tau and heparin in the absence (gray) and presence of 6 μM wt DNAJA2 or its S51 variants. Data shown in panels (a), (b), (d), and (e) are mean \pm s. d. of at least three independent experiments. G6PDH, glucose-6-phosphate dehydrogenase.

2.3 | Phosphorylated JDs recapitulate results from full-length phosphomimetic variants

We next wanted to test whether similar functional effects were induced by truly phosphorylated JDs. To this aim, three JDs (residues 1–78) were synthesized: wt JD and its phosphorylated variants JD-pY10 and JD-pS51 (Figure 4a). We first studied the ability of these peptides to activate Hsc70 in the presence of Apg2 and saturating concentrations (100 μM) of the peptide substrate FT7 (FYQLALT) (Figure 4b) (Takenaka et al., 1995). These conditions fully activated the chaperone and allowed a better comparison of the effect of the different JDs, although similar results were

obtained without Apg2 (Figure S3A in Data S1) or FT7 (Figure S3B in Data S1). Titration of Hsc70 with JD-pS51 showed that this variant did not stimulate Hsc70, in agreement with data shown above for DNAJA2-S51E (Figure 4b).

The activation extent of JD-pY10, relative to the wt JD, was reduced around 45% and 70% in the absence (Figure S3A in Data S1) and presence of Apg2 (Figure S3B in Data S1), respectively, and addition of FT7 to the ternary mixture did not significantly modify this value (65%; Figure 4b). This reduction was stronger than that found for full-length DNAJA2-Y10E (around 15%–22%; Figure 2a), suggesting that regions other than the JD might contribute to chaperone stimulation or that

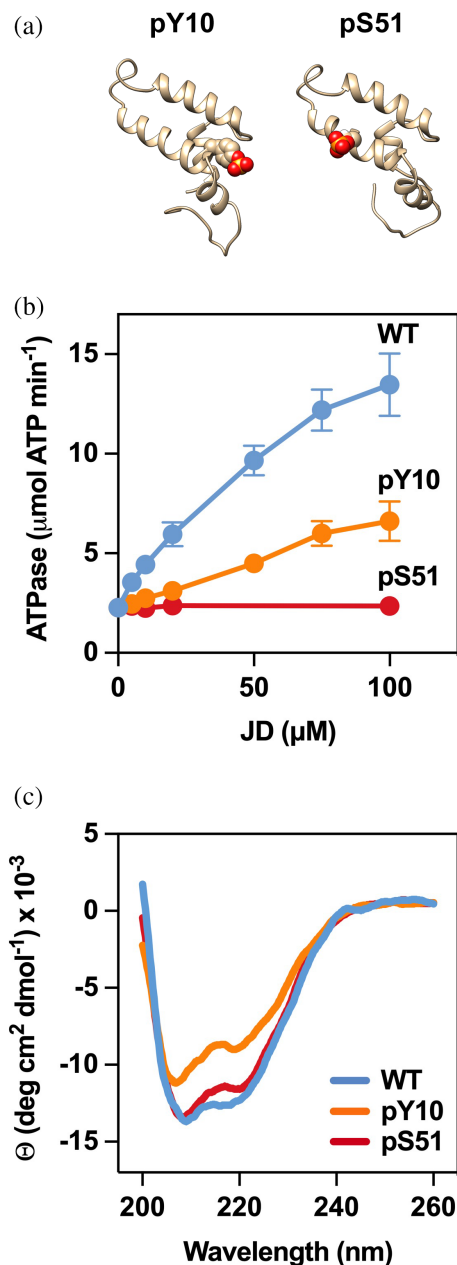


FIGURE 4 Effect of Y10 and S51 phosphorylation on the conformation of the JD and Hsc70 activation. (a) Location in the JD of the amino acids that were replaced by their phosphorylated counterparts. (b) Stimulation of the ATPase activity of 2 μM Hsc70 by increasing concentrations of wt JD (blue) or its phosphorylated variants JD-pY10 (orange) and JD-pS51 (red) in the presence of 0.4 μM Apg2 and 100 μM FT7. Data are mean ± s.d. of three independent experiments. (c) Far-UV CD spectra of wt JD and its phosphorylated variants (10 μM) in buffer 10 mM potassium phosphate, pH 7.6, containing 20% TFE. Color code as in panel (a). CD, circular dichroism; JD, J-domain.

the phosphoryl group induces a stronger effect than the replacement by glutamic acid. Interestingly, phosphorylation of Y10 partially destabilized the JD, as seen by the decreased ellipticity at 222 nm, whereas phosphorylation

of S51 did not change the helical content of the JD (Figure 4c), in accordance with data obtained for the corresponding phosphomimetic variants.

2.4 | Structural basis for the functional regulation of the Hsp70 system by J-domain phosphorylation

2.4.1 | Molecular dynamics (MD)

To provide a theoretical basis to the experimental data, we generated atomistic models of the JD of DNAJA2 (Figure 1b) and of the JD/Hsc70(ATP) complex (Figure S4 in Data S1) using as templates the structures of the JD of DNAJB1 (pdb code 1HDI) (Qian et al., 1996) and the JD of bacterial DnaJ in complex with DnaK (pdb code 5NRO) (Kityk et al., 2018). First, MD simulations of wt JD and its phosphorylated (JD-pY10 and JD-pS51) variants were carried out to predict phosphorylation-dependent conformational changes.

In the homology model of the wt JD, Y10 in helix I links this helical segment and helix IV through a H-bond network with R63 and D67 and Van der Waals contacts with Y66 (Figure 5a, left panel), in agreement with the structure of the JD of DNAJB1 (Qian et al., 1996). Upon phosphorylation, the phosphate group of pY10 established a strong electrostatic interaction with the side chain of R63, disrupting the interaction with Y66 and D67 in the C-terminal end of helix IV and weakening the H-bond between R63 and D67 (Figure 5a, right panel). These effects might destabilize helix IV. Although Y10 is situated on the opposite side of the interacting surface with Hsc70 in the model of the DNAJA2-JD/Hsc70 complex and does not directly interact with the chaperone (Figure S4 in Data S1), phosphorylation of Y10 could induce a structural rearrangement in helices I and IV. This rearrangement may modify the region responsible for Hsc70 binding—helices II and III and the connecting HPD loop—as previous studies have suggested (Cheetham and Caplan, 1998; Qian et al., 1996). The observed destabilization of the JD in JD-pY10 and in the phosphomimetic DNAJA2-Y10E variant (Figure 2e,f) together with its functional defects (Figure 2b,c) would support this interpretation.

Phosphorylation of S51 in helix III could weaken the H-bond that forms with Y28 in helix II (Figure 5b, left panel), the phosphate group forming instead a salt bridge with K48 also in helix III (Figure 5b, right panel). The predicted intramolecular pS51-K48 ionic contact could outcompete the interaction of K48 with D479 of Hsc70, which was observed in the bacterial system (K48 of DNAJ interacts with D477—D479 in Hsc70—of DnaK)

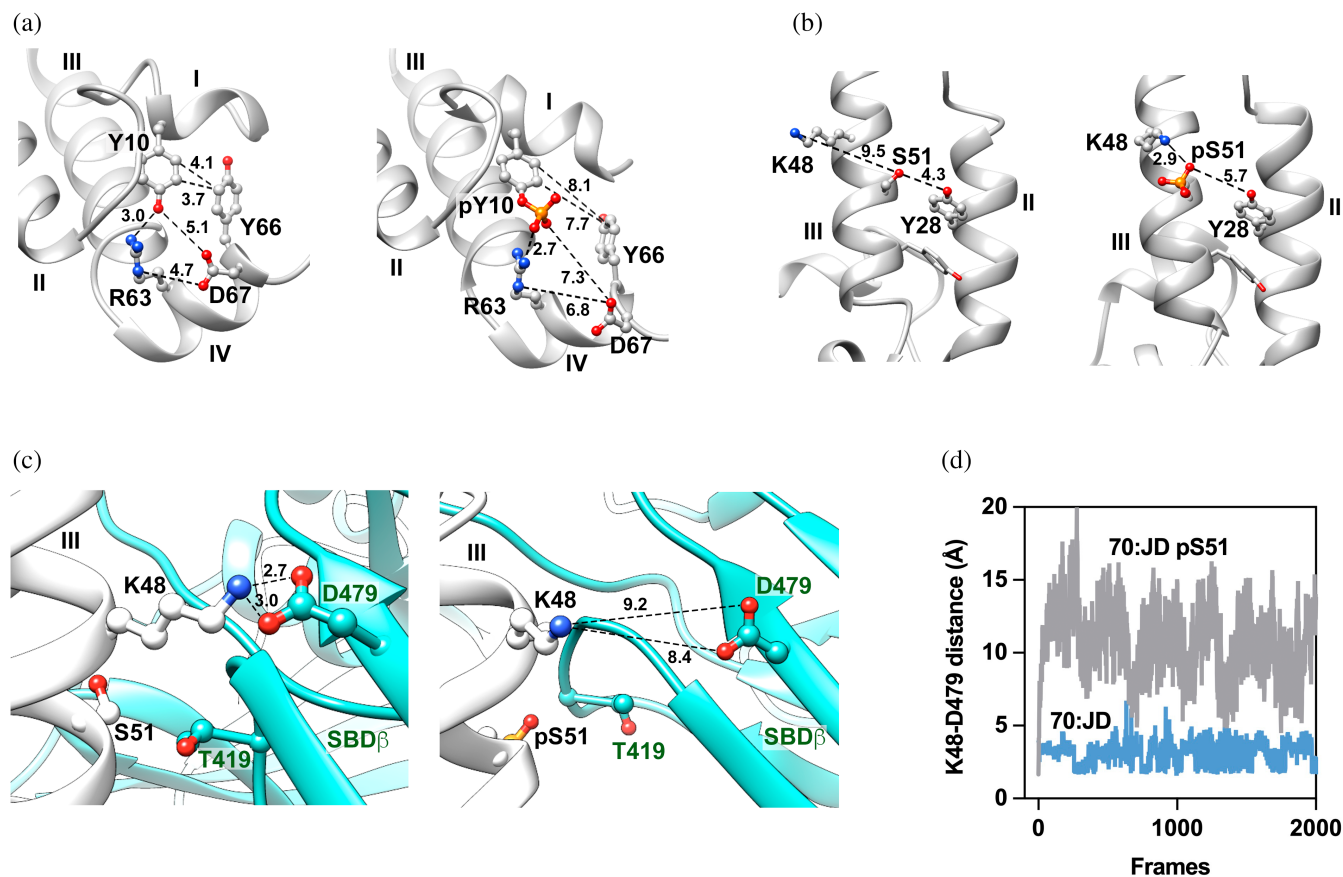


FIGURE 5 MD simulations of the effect of Y10 and S51 phosphorylation on JD conformation and interaction with Hsc70. (a) The most representative frame of wt JD (left panel) and JD-pY10 (right panel) after 300 ns MD. In wt JD, Y10 contacts R63, Y66, and D67 in helix IV of the JD. Upon phosphorylation, pY10 electrostatically interacts with R63. Distances between atoms are given in Å in all panels. (b) Representative frames of wt JD (left panel) and JD-pS51 (right panel) after 300 ns MD. S51 in helix III interacts with Y28 in helix II and upon phosphorylation with K48 (helix III). (c) The most representative frames of Hsc70 (light blue) in complex with wt JD (light gray; left panel) or JD-pS51 (right panel) showing the distances between the nitrogen of K48 in the JD and the oxygen atoms (OD1 and OD2) of Hsc70 D479. The side chains of K48 and D479 interact in the non-phosphorylated complex (left panel), and move away upon S51 phosphorylation (right panel). (d) Distance between the nitrogen of the side chain of K48 (in the JD) and the oxygen (OD2) of D479 of Hsc70 during MD simulations (50 ns) of the complexes between Hsc70 and wt JD (blue) or JD-pS51 (gray). JD, J-domain; MD, molecular dynamics.

(Kityk et al., 2018) (Figure 5c, left panel). Supporting this interpretation is the fact that during MD of the Hsc70/JD-pS51 complex, phosphorylated JD moved from the initial position characteristic of the wt complex to a distance compatible with the disruption of the ionic bond (Figure 5c, right panel; Figure 5d). This finding suggests that S51 phosphorylation may compromise the stability of the complex, consequently impacting its chaperone activity, in agreement with the experimental data.

Multiple sequence alignment of different JDs of human class A, B, and C JDPs (Figure S5 in Data S1) showed that whereas Y10 is conserved in both A and B classes and in many C class members, a strong difference is found at position S51. This residue is conserved in the three cytosolic human class A JDPs (DNAJA1, DNAJA2, and DNAJA4) and it is also present only in one class B JDP, DNAJB8, and four class C JDPs, DNAJC4, DNAJC16,

DNAJC17, and DNAJC30, while other class B and C members replace S51 by non-phosphorylatable residues. Conservation of a serine at this specific position in helix III does not seem to be related to the cellular localization of the JDPs. The conservation of S51 in cytosolic class A JDPs might suggest that phosphorylation of S51 could be a reversible switch to regulate the folding activity of the Hsc70 system assisted by these JDPs.

2.4.2 | Nuclear magnetic resonance (NMR)

Next, we studied in detail the effect of pseudophosphorylation on the structure of DNAJA2 JD and its complex with Hsc70 using NMR chemical shift perturbation (CSP) analyses. To this aim, constructs containing the JD and G/FR (residues 1–111) of the wt protein and its phosphomimetic

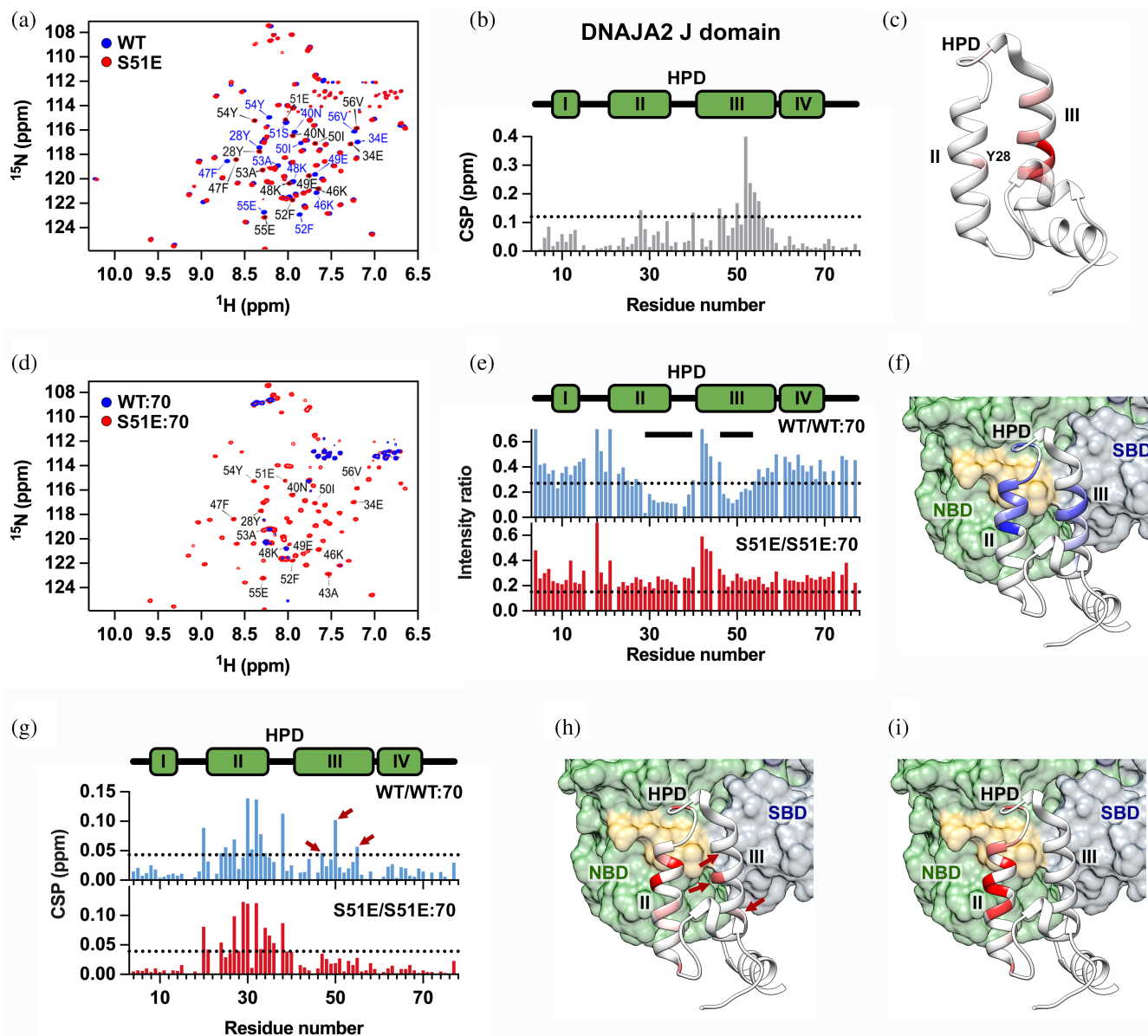


FIGURE 6 Pseudophosphorylation of S51 rearranges the cochaperone interaction surface and destabilizes the DNAJA2(JD-G/FR)-Hsc70 complex. (a) ^{15}N -HSQC spectra of wt (JD-G/FR) (blue) and (JD-G/FR)-S51E (red). Selected residues in helix II, helix III, and the connecting loop are indicated (see Figure S6A in Data S1 for the full assignment). Peaks altered in the spectrum of the mutant indicate changes in the chemical environment of the corresponding residues. (b) CSPs induced by the S51E mutation. The horizontal dotted line represents the threshold value ($2 \times \text{s.d.}$). (c) Mapping of the residues with CSP values above this value on the structure of the JD. They are highlighted in red, with the highest intensity corresponding to the largest perturbation. (d) ^{15}N -HSQC spectra of 0.2 mM wt (JD-G/FR) (blue) and (JD-G/FR)-S51E (red) in the presence of 0.2 mM Hsc70-T204A. Only residues with strong intensity changes are indicated (see Figure S6B in Data S1 for the full assignment). (e) Intensity ratio changes upon binding of wt (JD-G/FR) (blue) or (JD-G/FR)-S51E (red) to Hsc70-T204A. Reduction in intensity below the threshold value ($2 \times \text{s.d.}$; dotted line) indicates Hsc70 binding to these residues, which are located in regions of the wt protein marked with horizontal solid bars and are not detected in (JD-G/FR)-S51E. (f) Mapping of the residues showing a significant reduction in the intensity ratio (blue) on the structure of the wt JD-Hsc70 complex. (g) CSPs upon addition of equimolar amounts of Hsc70-T204A to 0.2 mM ^{15}N -labeled wt (JD-G/FR) (blue) or (JD-G/FR)-S51E (red). Dotted lines show the threshold values ($2 \times \text{s.d.}$) of each measurement. (h and i) Residues with CSPs values above these thresholds for wt (JD-G/FR) (h) or (JD-G/FR)-S51E (i) mapped on the structure of the JD. CSPs, chemical shift perturbations; JD, J-domain.

variants were analyzed. The same construct was recently used to study its interaction with Hsc70 by NMR (Faust et al., 2020). First, assignment of the backbone chemical shifts

of the wt construct was based on previous work (Faust et al., 2020) (Figure 6a, blue resonances, and Figure S6A in Data S1 for full assignments), and confirmed by HNC0,

HNCA, and HNCACB spectra. Unfortunately, we could not purify (JD-G/FR)-Y10E since it was severely proteolyzed under all conditions tested, which might be related to the JD destabilization observed above (Figure 2e,f). Doubly labeled ^{15}N and ^{13}C (JD-G/FR)-S51E was purified, and its secondary structure and global folding was checked by CD. The far-UV CD spectra (Figure S7A in Data S1) and thermal stability (Figure S7B in Data S1) of wt (JD-G/FR) and (JD-G/FR)-S51E, showing double minima at 208 and 222 nm characteristic of α -helical conformations and T_m values of 76°C, were virtually identical, indicating that the S51E substitution had negligible effects on the secondary structure and thermal stability of this construct.

The wt (JD-G/FR) dataset was used as reference for the phosphomimetic S51E variant (Figure 6a, red resonances). Data showed that S51E replacement induced shift changes in residues located in helix II (residues 28 and 34), the connecting loop (residue 40) and helix III (residues 46–56) (Figure 6b). It is worth noting the CSP observed for Y28 in helix II of the phosphomimetic variant, supporting that the interaction between S51 and Y28 in the non-phosphorylated protein could be modified in the pseudophosphorylated mutant (Figure 6b). The weak CSP detected for K48 also indicates that in contrast to what is expected for the lateral chain of this residue, which is predicted to electrostatically contact the phosphate group of S51, the chemical environment of its backbone NH group is only slightly perturbed in the phosphomimetic variant. The strongest CSPs observed for residues at helix III indicate that this helical segment, which hosts the mutation, specially senses the substitution (Figure 6c). The observed changes are large and spread way beyond the mutation site, suggesting that S51E replacement alters the chemical environment of JD residues that contact Hsc70 and thus, could regulate its interaction with the chaperone.

We then aimed to characterize the interaction of the (JD-G/FR) constructs with Hsc70 by NMR spectroscopy. The transient interplay between JDPs and Hsc70s complicates the analysis of their complexes. To overcome this limitation, we employed, as done recently (Faust et al., 2020), a chaperone mutant (Hsc70-T204A) with a 10-fold lower ATPase rate (Jiang et al., 2007) and an ATP-induced conformational rearrangement and response to JDPs comparable to the wt protein (Wu et al., 2020). The ^{15}N -HSQC spectra of wt (JD-G/FR) and (JD-G/FR)-S51E were recorded in the presence of equimolar amounts (0.2 mM) of Hsc70-T204A and 2 mM ATP (Figure 6d), and analyzed using the spectra obtained in the absence of the chaperone as reference (Figures 6a and S6B in Data S1). The interaction of wt (JD-G/FR) with Hsc70-T204A induced both changes in the correlation time that resulted in signal broadening with the

associated reduction of peak intensity of specific JD signals due to Hsc70 binding (Figure 6e, top), and CSPs (Figure 6g, top). Selective peak broadening was observed for residues located at the end of helix II (residues 29–35), the connecting loop containing the HPD motif (residues 36–39) and helix III (residues 47–53) (Figure 6e, top panel and Figure 6f), in agreement with previous studies (Faust et al., 2020). Of special interest in the context of this study are the resonances that behave distinctly in both constructs. The first difference is that interaction of (JD-G/FR)-S51E with the chaperone did not elicit significant intensity changes, even at the high protein concentration used (0.2 mM) (Figure 6e bottom, and Figure S6C in Data S1). CSPs caused by Hsc70 binding were observed for both JD-G/FR constructs in amino acids within helix II (residues 24–34) and the HPD motif (D38) (Figure 6g). This suggests that Hsc70 binding to (JD-G/FR)-S51E was in fast exchange, and therefore did not induce reduction in peak intensities (Faust et al., 2020). Notably, CSPs for residues within helix III were exclusively observed in wt (JD-G/FR) (residues 47, 50, and 55) (Figure 6g). This is better seen in Figure 6h,i, which revealed the disappearance of the anchor region of helix III with the SBD of Hsc70 upon S51 pseudophosphorylation. If a stable interaction of the essential HPD motif with Hsc70 requires contact of both flanking helical regions with the chaperone, the absence of one of them could result in the inability of the S51E variant to form stable, productive complexes with the chaperone.

3 | DISCUSSION

DNAJA2 is considered a potent holdase that efficiently suppresses or delays tau seeding and intracellular formation of amyloids (Mok et al., 2018) and also assists Hsc70 in substrate remodeling (Nillegoda et al., 2015). Most of the phosphorylated residues identified in members of class A JDPs have been described in harsh conditions (Hornbeck et al., 2015) and therefore could modulate the activity of the Hsp70 system under stress. Targeted regulation of the Hsp70 system via PTM of the JDP component would offer a significant advantage over modifying the central Hsc70, which is involved in a plethora of essential cellular functions. Modifying a specific JDP would exclusively impact the cellular processes in which is involved, potentially enhancing the regulation and functional specificity of the Hsc70 system.

In this study, we find that phosphorylation of specific residues of the DNAJA2 J domain (JD) possibly impairs the productive interaction with Hsc70. Comparison of the functional properties of DNAJA2-Y10E and DNAJA2-Y10A, indicates that the negative charge introduced by the

phosphomimetic mutation specifically induces a significant inhibition of the Hsc70 system refolding activity. Both mutations of Y10 to E or A and substitution by pY induce partial unfolding of the JD, evidenced by the decreased helical content compared with their wt counterparts. MD analysis suggests that Y10 phosphorylation in helix I induces formation of a new ionic contact between pY10 and R63 in helix IV. Modification of the helix I–helix IV interface might affect the overall fold of the JD, as the antiparallel coiled coil formed by helices II and III, which together with their connecting loop form the interacting surface with Hsc70, is further stabilized by helices I and IV (Cheetham and Caplan, 1998). This is in agreement with the loss of the transition above 60°C associated to JD unfolding. An order-to-disorder transition has also been observed for DNAJC5 (also termed cysteine string protein), a class C JDP, after phosphorylation of S10, which promotes a rearrangement of the protein structure through a new electrostatic interaction with K58 in the JD (Patel et al., 2016). Phosphorylation of DNAJC5 by cyclic AMP-dependent protein kinase causes the defective binding to two protein substrates involved in exocytosis, syntaxin, and synaptotagmin (Evans and Morgan, 2002; Evans et al., 2001). Instead, our data show that (pseudo)phosphorylation of Y10 in DNAJA2 impairs the productive interaction with Hsc70. In both cases, the phosphorylation-induced structural reorganization of the JD seeks to regulate the interaction of the JDP with its partners (clients for DNAJC5 or Hsc70 for DNAJA2).

Phosphorylation of S51 modulates the interaction with Hsc70 through a different mechanism that does not involve a large structural rearrangement of the JD. S51 (pseudo)phosphorylation completely inhibits the disaggregating and refolding activities of the Hsc70 system. MD suggests that phosphorylated S51 forms a salt bridge with K48 that could outcompete formation of the salt bridge between K48 and D479 at the SBD of Hsc70. Functional analysis performed with bacterial DnaK and DnaJ showed that mutation of DnaK D477 (D479 in Hsc70) to Ala does not complement the temperature-sensitivity of a Δ DnaK strain and that DnaJ(1–75)-K48A is unable to stimulate the ATPase activity of DnaK (Kityk et al., 2018), indicating that the K48(JD)-D477(SBD) interaction is essential for formation of a productive DnaJ-DnaK complex. Similarly, S51 phosphorylation-induced disruption of the K48-D479 link for the human chaperones, might weaken the complex between DNAJA2 and Hsc70. Indeed, the phosphomimetic S51E mutation abolishes the reduction in peak intensity observed in HSQC spectra in the presence of Hsc70 for residues in helix II (residues 31–34), in the loop containing the HPD motif (residues 35–38) and in helix III (residues 48–50) of wt DNAJA2 (Figure 6e). Persistence of CSPs in residues at helix II of (JD-G/F)-S51E, indicates

that it still transiently interacts with the NBD of Hsp70, but the loss of CSPs in helix III suggests that it loses the anchor with the chaperone SBD β (Figure 6g–i). These data suggest that (pseudo)phosphorylation at S51 modifies and weakens the binding of the JD to Hsc70, which might impede the stable interaction of the HPD motif with Hsc70, accounting for the functional defects observed (no ATPase activation, diminished recruitment of the chaperone to the aggregate surfaces, loss of the disaggregating/remodeling activity).

The interaction of JDPs with their Hsp70 partner is fine-tuned by the distribution of specific residues in the Hsp70 binding interface of the JD, particularly charged residues nearby the HDP motif within the JD (Delewski et al., 2016; Nillegoda et al., 2015; Schlenstedt et al., 1995; Zhang et al., 2023). The conservation of these residues within the JD has been proposed to build the discriminatory patterns that modulate JDP-JDP (Malinverni et al., 2023; Nillegoda and Bukau, 2015) and JDP-Hsp70 interactions (Malinverni et al., 2023; Zhang et al., 2023). Phosphorylation—or other PTM—of these discriminatory regions within JDs could further help to rewire JDP-Hsp70 interactions, thereby linking their specific pairing to distinct functions (Kostenko et al., 2014). Sequence comparison of J domains from class A, B, and C JDPs reveals that among the four phosphorylatable residues studied here, S51 in helix III could be a discriminatory element of cytosolic class A JDPs, as is present in all of them, and occasionally is also found in one class B, DNAJB8, and four class C proteins, DNAJC4, DNAJC16, DNAJC17, and DNAJC30. Interestingly, the serine at this specific position has been identified phosphorylated in HTP experiments for DNAJB8 (Wang et al., 2011) and DNAJC17 (Hornbeck et al., 2015). Moreover, the JD of DNAJB8, also considered a good suppressor of aggregation of poly-Q amyloidogenic proteins (Hageman et al., 2010), has been predicted to belong to class A JDPs by an automated classification scheme based on artificial neural networks (Malinverni et al., 2023). Taken together, our findings suggest that phosphorylation of S51 might function as a class-specific switch that regulates the interaction of class A JDPs with Hsc70 under harsh conditions.

Although changes in JDP concentration through transcription activation can reorganize the JDP-Hsp70 network (Finka et al., 2015; Mathangasinghe et al., 2021; Sterrenberg et al., 2011; Vonk et al., 2020), its complexity might also require specific sequences in the JDs to regulate JDP-Hsp70 assembly (Zhang et al., 2023). Our data show that phosphorylation of DNAJA2 JD impairs its productive interaction with Hsc70 without affecting the holding activity of the JDP, adding an additional layer of complexity to the regulation of the Hsc70 system.

Phosphorylation of a single residue as S51 by kinases activated by cellular stress, like mitogen-activated protein kinases (Cuenda and Sanz-Ezquerro, 2017; Kostenko et al., 2014), could function as a specific and reversible switch to potentiate holding of protein clients by a JDP under harsh conditions, in detriment of their folding, strictly dependent on the productive collaboration between the JDP and the Hsp70. Thus, phosphorylation of JDPs as DNAJA2 constitutes a fast and economical mechanism for the cells to ensure low levels of misfolded proteins under stress (de Graff et al., 2020; Lindquist and Kelly, 2011). Dephosphorylation would be an easy way to restore the holding/folding balance once the harsh conditions disappear.

A limitation of this study is that we characterize the effect of (pseudo)phosphorylation of single residues of the JD, despite the presence of multiple phosphorylation sites in JDPs. Different combinations of phosphorylated residues and/or different PTMs could further tune the association of JDPs with client proteins and Hsc70, and therefore the activity of the chaperone network. It is also conceivable that PTMs affecting Hsc70 and JDPs, which modulate their interaction, are co-regulated to finely adjust the functional outcome of the Hsp70 system (Mitchem et al., 2023). Despite these limitations, our findings underscore the significance of phosphorylation at key JD residues in JDPs as an important factor in regulating the delicate balance between cellular holding and folding activities.

4 | MATERIALS AND METHODS

4.1 | Cloning, expression, and purification of proteins

The cDNAs of Apg2 (HSPH2), Hsc70 (HSPA8), and DNAJA2 were obtained from Addgene (Hageman and Kampinga, 2009) and cloned into a pE-SUMO vector (LifeSensors, Malvern, USA). The deletion mutants DNAJA2 Δ J and (JD-G/FR), carrying the deletion of residues 1–74 and 112–412, respectively, were cloned by fusing two PCR fragments corresponding to the upstream and downstream sequences of these protein segments. The phosphomimetic DNAJA2 mutants containing a glutamic residue instead of the experimentally found phosphorylated residues and Hsc70-T204A were generated by site-directed mutagenesis using the QuickChange II XL kit (Agilent). The JD-G/FR variants wt and S51E used for NMR studies were obtained from cultures grown in M9 minimal medium supplemented with $^{15}\text{NH}_4\text{Cl}$ and $^{13}\text{C}_6$ -glucose (Cambridge Isotope, USA). JD peptides (residues 1–78) corresponding to the wt, unphosphorylated

domain, and phosphorylated at Y10 (pY10) or S51 (pS51), as well as peptide FT7 (FYQLALT), were synthesized (99% pure) by Proteogenix (Schiltigheim, France).

All mutants were verified by sequencing. Recombinant chaperones containing a tag with 6xHis and SUMO fused to the N-terminus were expressed in BL21 Rosetta or BL21 (DE3) CodonPlus cells and purified as described (Cabrera et al., 2019). Tau K18 C291A, C322A, P301L was cloned into a pNG2 vector, expressed in *E. coli* BL21 (DE3) cells and purified as reported (Barghorn et al., 2005).

4.2 | ATPase assay

The ATPase activity of the samples was measured as described (Norby, 1988). Experiments were performed in a Synergy HXT plate reader (BioTek) at 30°C in 40 mM Hepes pH 7.6, 50 mM KCl, 5 mM magnesium acetate and 2 mM DTT buffer. Protein concentrations were 2 μM Hsc70, 0.4 μM Apg2, and 0.5 μM or increasing concentrations of JDPs. The ATPase-regeneration system (0.3 mM NADH, 3 mM phosphoenolpyruvate [PEP], 20 ng/mL pyruvate kinase [PK], 0.017 mg/mL lactate dehydrogenase and 2 mM ATP) was added to initiate the reaction. ATP consumption rates ($\mu\text{mol ATP min}^{-1}$) were calculated from the linear slopes of the A_{340} decay curves using the extinction coefficient of NADH (ϵ_{340} 6220 $\text{M}^{-1} \text{cm}^{-1}$).

4.3 | Holding activity

The aggregation of tau K18 P301L was monitored for 16 h at 37°C in a Synergy HTX plate reader (BioTek) using transparent 96-well plates with flat bottom (Sarstedt), recording the light scattered at 350 nm every 5 min. This truncated variant of tau (residues 244–372) contains the aggregation-prone repeats and the missense mutation P301L that has been linked to familial frontotemporal dementia, and aggregates faster than the wt, full-length protein (Gustke et al., 1994; Ingram and Spillantini, 2002). Samples were prepared by adding 6 μM of the DNAJA2 variants to mixtures of equimolar amounts (20 μM) of tau K18 P301L and heparin (MP Biomedicals) in buffer containing 25 mM Tris-HCl, pH 7.5, 200 mM NaCl, and 2 mM DTT.

4.4 | Refolding of unfolded luciferase: folding activity

Firefly luciferase (10 μM) (Sigma-Aldrich) was incubated at 30°C for 30 min in denaturation buffer (6 M urea,

40 mM Hepes, 50 mM KCl, 5 mM MgCl₂, 2 mM DTT, pH 7.6). Aggregation was induced by 100-fold dilution of unfolded luciferase into refolding buffer (40 mM Hepes, 50 mM KCl, 5 mM MgCl₂, 2 mM DTT, pH 7.6, 2 mM ATP, 3 mM PEP, 20 ng/mL PK) without (control) or with 1 μM JDP. Samples were supplied with 2 μM Hsc70 and 0.4 μM Apg2. Luciferase (0.1 μM) recovery was measured after 120 min at 30°C by adding 5 μL of each sample to 50 μL Luciferase Assay System (Promega, E1500) and recording the luminescence in a Synergy HTX plate reader (BioTeK) using white 96-well plates with flat bottoms (Sarstedt). When required, samples containing phosphomimetic mutants were supplied with 1 μM wt DNAJA2, to distinguish the holding and folding activities. The activity of non-denatured luciferase in the presence of the ternary chaperone mixture was set as 100%.

4.5 | Disaggregase activity

Recombinant luciferase from *P. pyralis* (Sigma-Aldrich) and G6PDH from *Leuconostoc mesenteroides* (Worthington) were aggregated and reactivated by the Hsc70 system as in previous works (Cabrera et al., 2019). Reactivation percentages were calculated considering the activity of the native proteins in the presence of chaperones proteins as 100%.

4.6 | Chaperone binding to G6PDH aggregates

The interaction between chaperones and G6PDH aggregates was followed with a co-sedimentation assay previously described (Cabrera et al., 2019). Briefly, aggregation of G6PDH (10 μM) was induced by incubation at 50°C for 30 min. Then, G6PDH aggregates were incubated at 30°C for 10 min and diluted to 0.4 μM in refolding buffer (40 mM Hepes, pH 7.6, 50 mM KCl, 5 mM MgCl₂, 2 mM DTT, 2 μM ATP, 8 μM PEP, 20 ng/mL PK) containing 2 μM Hsc70, 1 μM DNAJA2 or the corresponding mutant, and 0.4 μM Apg2. Samples were incubated for 10 min at 30°C and centrifuged at 55,000 rpm in a Beckman TLA-55 rotor. Supernatants were discarded and pellets were analyzed by SDS-PAGE and quantified by densitometry. The amount of aggregate-bound JDP and Hsc70, relative to that of aggregated G6PDH, was estimated by measuring the intensity of the corresponding bands using a gel scanner G-800 and the Quantity One software (Bio-Rad). Each data point is the average of at least three independent experiments and was assessed by subtracting the amount of protein found in pellets of control experiments, containing native G6PDH, which were carried out in parallel.

4.7 | Circular dichroism (CD)

Samples were prepared at 15 μM protein in 10 mM potassium phosphate, pH 7.6, and far-UV CD spectra (200–260 nm range) were acquired at 20°C in a Jasco J-810 CD spectropolarimeter using rectangular quartz cuvettes with 1 mm path length. Each spectrum represents the average of 15 scans, with a spectral bandwidth of 1 nm and a response time of 1 s. For thermal unfolding studies, the ellipticity at 222 nm was followed from 20 to 90°C with a heating rate of 1°C/min. The far-UV CD spectra of phosphorylated JDs (15 μM) were recorded in 10 mM potassium phosphate, pH 7.6, 20% TFE.

4.8 | NMR

All NMR experiments were carried out on a Bruker Advance III spectrometer operating at 18.8 T (800 MHz ¹H Larmor frequency). The HSQC spectra of 200 μM wt (JD-G/FR) and (JD-G/FR)-S51E were recorded at 25°C in 50 mM Hepes, 50 mM KCl, 5 mM MgCl₂, 2 mM DTT, 10% (v/v) D₂O, pH 7.6. They were also acquired in the presence of 100 μM or 200 μM Hsc70-T204A, 2 mM ATP, 3 mM PEP, and 20 ng/mL PK in the above buffer. These experimental conditions allow the interaction of both proteins at a constant ATP concentration during the time required to complete the measurement (120 min). ¹⁵N-HSQC, ¹³C-HSQC, HNC0, HNCA, and HNCACB spectra were first used to confirm the backbone assignments of the (JD-G/FR) constructs (Faust et al., 2020). The interaction of each construct with Hsc70-T204A was monitored by ¹⁵N-HSQC. HSQC spectra were processed with Topspin 3.2 (Bruker) and analyzed using in-house MATLAB scripts (Gunther et al., 2000) and CCPN software (Skinner et al., 2015). CSPs were calculated as follows:

$$\Delta\delta_{\text{total}} (\text{ppm}) = \sqrt{(\Delta\delta_{\text{H}})^2 + (0.2 \cdot \Delta\delta_{\text{N}})^2},$$

and analyzed as described (Ma et al., 2016).

4.9 | Homology modeling, MD simulations, and docking

We resorted to homology modeling to generate an atomistic model of DNAJA2. The first step was to search for the best templates by scanning the query sequence against SWISS-MODEL (Biasini et al., 2014), Phyre2 (Kelley et al., 2015), and I-TASSER (Roy et al., 2010) servers. Then, the templates were aligned with the query protein considering the structure, and the structure-based

alignment was used to generate the model using MODELLER (Webb and Sali, 2014). Different models were generated and all of them were analyzed by ERRAT (Colovos and Yeates, 1993), Verify-3D (Eisenberg et al., 1997), and WHAT-IF (Vriend, 1990) to assess their quality. The best model was selected, energy minimized, and refined by MD simulations using OMMProtocol as a command line application to launch MD simulations with OpenMM (Eastman and Pande, 2015). The structure of the model was similar to that obtained by Alphafold (ID AF-O60884-F1) (Jumper et al., 2021; Velasco-Carneros et al., 2023).

The systems (wt JD and its phosphorylated variants, and Hsc70(ATP)-DNAJA2 JD wt or pS51 complexes) were prepared for all-atom MD simulations as follows: histidines predicted to be in a region with $\text{pH} > 6.0$ by H^{++} server (Anandakrishnan et al., 2012) were protonated, and the system was set up with xleap. Explicit solvent was used and Na^+ or Cl^- ions were added to attain charge neutrality. The model system was embedded with a distance between the protein and the box edge of 6 Å. AMBER ff14SB (Maier et al., 2015) and TIP3P (Jorgensen et al., 1983) force fields were used for proteins and water, respectively. Parameters for the ZFDs were developed according to standard approaches (Peters et al., 2010).

MD simulations were performed using OpenMM (Eastman and Pande, 2015) with the following conditions: a cutoff of 1 nm was used for short range electrostatics and Van der Waals interactions. Long-range electrostatic interactions were calculated with the Particle-Mesh Ewald method, using periodic boundary conditions (Petersen, 1995). Bonds involving hydrogen atoms were constrained using the SHAKE algorithm (Ryckaert et al., 1977). A time step of 1 fs was used to integrate the equation of motion with a Langevin integrator (Brunger et al., 1984). Constant temperature and pressure were achieved by coupling the systems to a Monte Carlo barostat at 1.01325 bar (Duane et al., 1987). Model systems were energy minimized progressively before starting the MD simulations. Then, the temperature was increased from 100 to 300 K to achieve the thermalization of water molecules and side chains, and finally 300 ns MD simulations were carried out and further analyzed. The UCSF Chimera package was used for visualization and molecular graphics (Pettersen et al., 2004).

4.10 | Statistical analysis

Statistical analysis was performed in GraphPad Prism 9.3.1 using a two-tailed, one-way analysis of variance (ANOVA) and Tukey's multiple comparison test. The p values obtained with this analysis are shown in the

corresponding figures. A value of $p < 0.05$ was considered statistically significant.

AUTHOR CONTRIBUTIONS

Lorea Velasco-Carneros: Investigation; methodology; formal analysis. **Ganeko Bernardo-Seisedos:** Investigation; methodology. **Jean-Didier Maréchal:** Methodology; formal analysis. **Oscar Millet:** Investigation; methodology; formal analysis. **Fernando Moro:** Formal analysis; project administration; writing – review and editing; funding acquisition. **Arturo Muga:** Conceptualization; methodology; formal analysis; writing – review and editing; writing – original draft; funding acquisition; supervision; resources; data curation.

ACKNOWLEDGMENTS

We would like to thank Dr. J.M. Valpuesta for critically reading the manuscript. LV-C thanks the University of the Basque Country for a predoctoral fellowship. In loving memory of Arturo Muga, our close colleague and friend.

FUNDING INFORMATION

This research was supported by grants PID2019-111068GB-I00 (MICIU/AEI/10.13039/501100011033) to AM and FM, and IT1745-22 (Basque Government) to FM.

CONFLICT OF INTEREST STATEMENT

The authors declare no conflicts of interest.

ORCID

Arturo Muga  <https://orcid.org/0000-0003-0345-6882>

REFERENCES

- Ahmad A, Bhattacharya A, McDonald RA, Cordes M, Ellington B, Bertelsen EB, et al. Heat shock protein 70 kDa chaperone/DnaJ cochaperone complex employs an unusual dynamic interface. *Proc Natl Acad Sci USA*. 2011;108:18966–71.
- Anandakrishnan R, Aguilar B, Onufriev AV. H^{++} 3.0: automating pK prediction and the preparation of biomolecular structures for atomistic molecular modeling and simulations. *Nucleic Acids Res*. 2012;40:W537–41.
- Bachman AB, Keramisanou D, Xu W, Beebe K, Moses MA, Vasantha Kumar MV, et al. Phosphorylation induced cochaperone unfolding promotes kinase recruitment and client class-specific Hsp90 phosphorylation. *Nat Commun*. 2018;9:265.
- Backe SJ, Sager RA, Woodford MR, Makedon AM, Mollapour M. Post-translational modifications of Hsp90 and translating the chaperone code. *J Biol Chem*. 2020;295:11099–117.
- Barghorn S, Biernat J, Mandelkow E. Purification of recombinant tau protein and preparation of Alzheimer-paired helical filaments in vitro. *Methods Mol Biol*. 2005;299:35–51.
- Barriot R, Latour J, Castanie-Cornet MP, Fichant G, Genevaux P. J-domain proteins in bacteria and their viruses. *J Mol Biol*. 2020;432:3771–89.

- Beebe K, Mollapour M, Scroggins B, Prodromou C, Xu W, Tokita M, et al. Posttranslational modification and conformational state of heat shock protein 90 differentially affect binding of chemically diverse small molecule inhibitors. *Oncotarget*. 2013;4:1065–74.
- Biasini M, Bienert S, Waterhouse A, Arnold K, Studer G, Schmidt T, et al. SWISS-MODEL: modelling protein tertiary and quaternary structure using evolutionary information. *Nucleic Acids Res*. 2014;42:W252–8.
- Brehme M, Voisine C, Rolland T, Wachi S, Soper JH, Zhu Y, et al. A chaperome subnetwork safeguards proteostasis in aging and neurodegenerative disease. *Cell Rep*. 2014;9:1135–50.
- Brunger A, Brooks CL, Karplus M. Stochastic boundary-conditions for molecular-dynamics simulations of ST2 water. *Chem Phys Lett*. 1984;105:495–500.
- Cabrera Y, Dublang L, Fernandez-Higuero JA, Albesa-Jove D, Lucas M, Viguera AR, et al. Regulation of human Hsc70 ATPase and chaperone activities by Apg2: role of the acidic subdomain. *J Mol Biol*. 2019;431:444–61.
- Cabrera Y, Bernardo-Seisdedos G, Dublang L, Albesa-Jove D, Orozco N, Viguera AR, et al. Fine-tuning of the Hsc70-based human protein disaggregase machinery by the distinctive C-terminal extension of Apg2. *J Mol Biol*. 2022;434:167841.
- Cheetham ME, Caplan AJ. Structure, function and evolution of DnaJ: conservation and adaptation of chaperone function. *Cell Stress Chaperones*. 1998;3:28–36.
- Cloutier P, Coulombe B. Regulation of molecular chaperones through post-translational modifications: decrypting the chaperone code. *Biochim Biophys Acta*. 2013;1829:443–54.
- Colovos C, Yeates TO. Verification of protein structures: patterns of nonbonded atomic interactions. *Protein Sci*. 1993;2:1511–9.
- Craig EA, Marszalek J. How do J-proteins get Hsp70 to do so many different things? *Trends Biochem Sci*. 2017;42:355–68.
- Cuenda A, Sanz-Ezquerro JJ. p38 γ and p38 δ : from spectators to key physiological players. *Trends Biochem Sci*. 2017;42:431–42.
- Dekker SL, Kampinga HH, Bergink S. DNAJs: more than substrate delivery to HSPA. *Front Mol Biosci*. 2015;2:35.
- Delewski W, Paterkiewicz B, Manicki M, Schilke B, Tomiczek B, Ciesielski SJ, et al. Iron-sulfur cluster biogenesis chaperones: evidence for emergence of mutational robustness of a highly specific protein-protein interaction. *Mol Biol Evol*. 2016;33:643–56.
- Duane S, Kennedy AD, Pendleton BJ, Roweth D. Hybrid Monte-Carlo. *Phys Lett B*. 1987;195:216–22.
- Eastman P, Pande VS. OpenMM: a hardware independent framework for molecular simulations. *Comput Sci Eng*. 2015;12:34–9.
- Eisenberg D, Luthy R, Bowie JU. VERIFY3D: assessment of protein models with three-dimensional profiles. *Methods Enzymol*. 1997;277:396–404.
- Evans GJ, Morgan A. Phosphorylation-dependent interaction of the synaptic vesicle proteins cysteine string protein and synaptotagmin I. *Biochem J*. 2002;364:343–7.
- Evans GJ, Wilkinson MC, Graham ME, Turner KM, Chamberlain LH, Burgoyne RD, et al. Phosphorylation of cysteine string protein by protein kinase A: implications for the modulation of exocytosis. *J Biol Chem*. 2001;276:47877–85.
- Faust O, Abayev-Avraham M, Wentink AS, Maurer M, Nilleghoda NB, London N, et al. HSP40 proteins use class-specific regulation to drive HSP70 functional diversity. *Nature*. 2020;587:489–94.
- Fernandez-Fernandez MR, Valpuesta JM. Hsp70 chaperone: a master player in protein homeostasis. *F1000Res*. 2018;7:7.
- Finka A, Sood V, Quadroni M, Rios Pde L, Goloubinoff P. Quantitative proteomics of heat-treated human cells show an across-the-board mild depletion of housekeeping proteins to massively accumulate few HSPs. *Cell Stress Chaperones*. 2015;20:605–20.
- de Graff AM, Mosedale DE, Sharp T, Dill KA, Grainger DJ. Proteostasis is adaptive: balancing chaperone holdases against foldases. *PLoS Comput Biol*. 2020;16:e1008460.
- Gunther UL, Ludwig C, Ruterjans H. NMR-LAB-advanced NMR data processing in matlab. *J Magn Reson*. 2000;145:201–8.
- Guo K, Wang YP, Zhou ZW, Jiang YB, Li W, Chen XM, et al. Impact of phosphomimetic and non-phosphorylatable mutations of phospholemman on L-type calcium channels gating in HEK 293T cells. *J Cell Mol Med*. 2015;19:642–50.
- Gustke N, Trinczek B, Biernat J, Mandelkow EM, Mandelkow E. Domains of tau protein and interactions with microtubules. *Biochemistry*. 1994;33:9511–22.
- Hageman J, Kampinga HH. Computational analysis of the human HSPH/HSPA/DNAJ family and cloning of a human HSPH/HSPA/DNAJ expression library. *Cell Stress Chaperones*. 2009;14:1–21.
- Hageman J, Rujano MA, van Waarde MA, Kakkar V, Dirks RP, Govorukhina N, et al. A DNAJB chaperone subfamily with HDAC-dependent activities suppresses toxic protein aggregation. *Mol Cell*. 2010;37:355–69.
- Hipp MS, Kasturi P, Hartl FU. The proteostasis network and its decline in ageing. *Nat Rev Mol Cell Biol*. 2019;20:421–35.
- Hornbeck PV, Zhang B, Murray B, Kornhauser JM, Latham V, Skrzypek E. PhosphoSitePlus, 2014: mutations, PTMs and recalibrations. *Nucleic Acids Res*. 2015;43:D512–20.
- Ingram EM, Spillantini MG. Tau gene mutations: dissecting the pathogenesis of FTDP-17. *Trends Mol Med*. 2002;8:555–62.
- Jayaraj GG, Hipp MS, Hartl FU. Functional modules of the proteostasis network. *Cold Spring Harb Perspect Biol*. 2020;12:a033951.
- Jiang J, Maes EG, Taylor AB, Wang L, Hinck AP, Lafer EM, et al. Structural basis of J cochaperone binding and regulation of Hsp70. *Mol Cell*. 2007;28:422–33.
- Jorgensen WL, Chandrasekhar J, Madura JD, Impey RW, Klein ML. Comparison of simple potential functions for simulating liquid water. *J Chem Phys*. 1983;79:926–35.
- Jumper J, Evans R, Pritzel A, Green T, Figurnov M, Ronneberger O, et al. Highly accurate protein structure prediction with AlphaFold. *Nature*. 2021;596:583–9.
- Kampinga HH, Craig EA. The HSP70 chaperone machinery: J proteins as drivers of functional specificity. *Nat Rev Mol Cell Biol*. 2010;11:579–92.
- Kao CH, Ryu SW, Kim MJ, Wen X, Wimalarathne O, Paull TT. Growth-regulated Hsp70 phosphorylation regulates stress responses and prion maintenance. *Mol Cell Biol*. 2020;40:e00628-19.
- Kelley LA, Mezulis S, Yates CM, Wass MN, Sternberg MJ. The Pyre2 web portal for protein modeling, prediction and analysis. *Nat Protoc*. 2015;10:845–58.
- Kettenbach AN, Schweppe DK, Faherty BK, Pechenick D, Pletnev AA, Gerber SA. Quantitative phosphoproteomics identifies substrates and functional modules of Aurora and polo-like kinase activities in mitotic cells. *Sci Signal*. 2011;4:rs5.

- Kirstein J, Arnsburg K, Scior A, Szlachcic A, Guilbride DL, Morimoto RI, et al. In vivo properties of the disaggregase function of J-proteins and Hsc70 in *Caenorhabditis elegans* stress and aging. *Aging Cell*. 2017;16:1414–24.
- Kityk R, Kopp J, Mayer MP. Molecular mechanism of J-domain-triggered ATP hydrolysis by Hsp70 chaperones. *Mol Cell*. 2018;69(2):227–237.e4.
- Kleczewska M, Grabinska A, Jelen M, Stolarska M, Schilke B, Marszalek J, et al. Biochemical convergence of mitochondrial Hsp70 system specialized in iron-sulfur cluster biogenesis. *Int J Mol Sci*. 2020;21:3326.
- Kostenko S, Jensen KL, Moens U. Phosphorylation of heat shock protein 40 (Hsp40/DnaJ1) by mitogen-activated protein kinase-activated protein kinase 5 (MK5/PRAK). *Int J Biochem Cell Biol*. 2014;47:29–37.
- Labbadia J, Morimoto RI. The biology of proteostasis in aging and disease. *Annu Rev Biochem*. 2015;84:435–64.
- Lindquist SL, Kelly JW. Chemical and biological approaches for adapting proteostasis to ameliorate protein misfolding and aggregation diseases: progress and prognosis. *Cold Spring Harb Perspect Biol*. 2011;3:3.
- Liu Q, Liang C, Zhou L. Structural and functional analysis of the Hsp70/Hsp40 chaperone system. *Protein Sci*. 2020;29:378–90.
- Ma LC, Guan R, Hamilton K, Aramini JM, Mao L, Wang S, et al. A second RNA-binding site in the NS1 protein of influenza B virus. *Structure*. 2016;24:1562–72.
- Maier JA, Martinez C, Kasavajhala K, Wickstrom L, Hauser KE, Simmerling C. ff14SB: improving the accuracy of protein side chain and backbone parameters from ff99SB. *J Chem Theory Comput*. 2015;11:3696–713.
- Malinverni D, Jost Lopez A, De Los RP, Hummer G, Barducci A. Modeling Hsp70/Hsp40 interaction by multi-scale molecular simulations and coevolutionary sequence analysis. *elife*. 2017;6:6.
- Malinverni D, Zamuner S, Rebeaud ME, Barducci A, Nillegoda NB, De Los RP. Data-driven large-scale genomic analysis reveals an intricate phylogenetic and functional landscape in J-domain proteins. *Proc Natl Acad Sci USA*. 2023;120:e2218217120.
- Mathangasinghe Y, Fauvet B, Jane SM, Goloubinoff P, Nillegoda NB. The Hsp70 chaperone system: distinct roles in erythrocyte formation and maintenance. *Haematologica*. 2021;106:1519–34.
- Mertins P, Yang F, Liu T, Mani DR, Petyuk VA, Gillette MA, et al. Ischemia in tumors induces early and sustained phosphorylation changes in stress kinase pathways but does not affect global protein levels. *Mol Cell Proteomics*. 2014;13:1690–704.
- Mitchem MM, Shrader C, Abedi E, Truman AW. Novel insights into the post-translational modifications of Ydj1/DNAJA1 co-chaperones. *Cell Stress Chaperones*. 2023;29:1–9.
- Mok SA, Condello C, Freilich R, Gillies A, Arhar T, Oroz J, et al. Mapping interactions with the chaperone network reveals factors that protect against tau aggregation. *Nat Struct Mol Biol*. 2018;25:384–93.
- Morishima Y, Mehta RK, Yoshimura M, Lau M, Southworth DR, Lawrence TS, et al. Chaperone activity and dimerization properties of Hsp90alpha and Hsp90beta in glucocorticoid receptor activation by the multiprotein Hsp90/Hsp70-dependent chaperone machinery. *Mol Pharmacol*. 2018;94:984–91.
- Muhlhofer M, Peters C, Kriehuber T, Kreuzeder M, Kazman P, Rodina N, et al. Phosphorylation activates the yeast small heat shock protein Hsp26 by weakening domain contacts in the oligomer ensemble. *Nat Commun*. 2021;12:6697.
- Nillegoda NB, Bukau B. Metazoan Hsp70-based protein disaggregases: emergence and mechanisms. *Front Mol Biosci*. 2015;2:57.
- Nillegoda NB, Kirstein J, Szlachcic A, Berynsky M, Stank A, Stengel F, et al. Crucial HSP70 co-chaperone complex unlocks metazoan protein disaggregation. *Nature*. 2015;524:247–51.
- Nitika PCM, Truman AW, Truttman MC. Post-translational modifications of Hsp70 family proteins: expanding the chaperone code. *J Biol Chem*. 2020;295:10689–708.
- Norby JG. Coupled assay of Na⁺,K⁺-ATPase activity. *Methods Enzymol*. 1988;156:116–9.
- Omkar S, Rysbayeva A, Truman AW. Understanding chaperone specificity: evidence for a ‘client code’. *Trends Biochem Sci*. 2023;48:662–4.
- Patel P, Prescott GR, Burgoyne RD, Lian LY, Morgan A. Phosphorylation of cysteine string protein triggers a major conformational switch. *Structure*. 2016;24:1380–6.
- Perez-Mejias G, Velazquez-Cruz A, Guerra-Castellano A, Banos-Jaime B, Diaz-Quintana A, Gonzalez-Arzola K, et al. Exploring protein phosphorylation by combining computational approaches and biochemical methods. *Comput Struct Biotechnol J*. 2020;18:1852–63.
- Peters MB, Yang Y, Wang B, Fusti-Molnar L, Weaver MN, Merz KM Jr. Structural survey of zinc containing proteins and the development of the zinc AMBER force field (ZAFF). *J Chem Theory Comput*. 2010;6:2935–47.
- Petersen HG. Accuracy and efficiency of the particle mesh Ewald method. *J Chem Phys*. 1995;103:3668–79.
- Pettersen EF, Goddard TD, Huang CC, Couch GS, Greenblatt DM, Meng EC, et al. UCSF chimera—a visualization system for exploratory research and analysis. *J Comput Chem*. 2004;25:1605–12.
- Qian YQ, Patel D, Hartl FU, McColl DJ. Nuclear magnetic resonance solution structure of the human Hsp40 (HDJ-1) J-domain. *J Mol Biol*. 1996;260:224–35.
- Rosenzweig R, Nillegoda NB, Mayer MP, Bukau B. The Hsp70 chaperone network. *Nat Rev Mol Cell Biol*. 2019;20:665–80.
- Roy A, Kucukural A, Zhang Y. I-TASSER: a unified platform for automated protein structure and function prediction. *Nat Protoc*. 2010;5:725–38.
- Ryckaert JP, Ciccotti G, Berendsen HJC. Numerical-integration of Cartesian equations of motion of a system with constraints – molecular-dynamics of N-alkanes. *J Comput Phys*. 1977;23:327–41.
- Schlenstedt G, Harris S, Risse B, Lill R, Silver PA. A yeast DnaJ homologue, Scj1p, can function in the endoplasmic reticulum with BiP/Kar2p via a conserved domain that specifies interactions with Hsp70s. *J Cell Biol*. 1995;129:979–88.
- Skinner SP, Goult BT, Fogh RH, Boucher W, Stevens TJ, Laue ED, et al. Structure calculation, refinement and validation using *CcpNmr Analysis*. *Acta Crystallogr D Biol Crystallogr*. 2015;71:154–61.
- Stateva SR, Salas V, Benaim G, Menendez M, Solis D, Villalobo A. Characterization of phospho-(tyrosine)-mimetic calmodulin mutants. *PLoS One*. 2015;10:e0120798.
- Sterrenberg JN, Blatch GL, Edkins AL. Human DNAJ in cancer and stem cells. *Cancer Lett*. 2011;312:129–42.

- Subramanyam S, Ismail M, Bhattacharya I, Spies M. Tyrosine phosphorylation stimulates activity of human RAD51 recombinase through altered nucleoprotein filament dynamics. *Proc Natl Acad Sci USA*. 2016;113:E6045–54.
- Takenaka IM, Leung SM, McAndrew SJ, Brown JP, Hightower LE. Hsc70-binding peptides selected from a phage display peptide library that resemble organellar targeting sequences. *J Biol Chem*. 1995;270:19839–44.
- Tomiczek B, Delewski W, Nierzwicki L, Stolarska M, Grochowina I, Schilke B, et al. Two-step mechanism of J-domain action in driving Hsp70 function. *PLoS Comput Biol*. 2020;16:e1007913.
- Truman AW, Bourboullia D, Mollapour M. Decrypting the chaperone code. *J Biol Chem*. 2021;296:100293.
- Tsai CF, Wang YT, Yen HY, Tsou CC, Ku WC, Lin PY, et al. Large-scale determination of absolute phosphorylation stoichiometries in human cells by motif-targeting quantitative proteomics. *Nat Commun*. 2015;6:6622.
- Velasco L, Dublang L, Moro F, Muga A. The complex phosphorylation patterns that regulate the activity of Hsp70 and its co-chaperones. *Int J Mol Sci*. 2019;20:4122.
- Velasco-Carneros L, Cuellar J, Dublang L, Santiago C, Marechal JD, Martin-Benito J, et al. The self-association equilibrium of DNAJA2 regulates its interaction with unfolded substrate proteins and with Hsc70. *Nat Commun*. 2023;14:5436.
- Vonk WIM, Rainbolt TK, Dolan PT, Webb AE, Brunet A, Frydman J. Differentiation drives widespread rewiring of the neural stem cell chaperone network. *Mol Cell*. 2020;78(2):329–345.e9.
- Vriend G. WHAT IF: a molecular modeling and drug design program. *J Mol Graph*. 1990;8(1):52–6.
- Wang Y, Yang F, Fu Y, Huang X, Wang W, Jiang X, et al. Spatial phosphoprotein profiling reveals a compartmentalized extracellular signal-regulated kinase switch governing neurite growth and retraction. *J Biol Chem*. 2011;286:18190–201.
- Webb B, Sali A. Comparative protein structure modeling using MODELLER. *Curr Protoc Bioinformatics*. 2014;47:5.6.1–5.6.32.
- Wu S, Hong L, Wang Y, Yu J, Yang J, Yang J, et al. Kinetics of the conformational cycle of Hsp70 reveals the importance of the dynamic and heterogeneous nature of Hsp70 for its function. *Proc Natl Acad Sci USA*. 2020;117:7814–23.
- Zhang R, Malinverni D, Cyr DM, Rios PL, Nillegoda NB. J-domain protein chaperone circuits in proteostasis and disease. *Trends Cell Biol*. 2023;33:30–47.

SUPPORTING INFORMATION

Additional supporting information can be found online in the Supporting Information section at the end of this article.

How to cite this article: Velasco-Carneros L, Bernardo-Seisdedos G, Maréchal J-D, Millet O, Moro F, Muga A. Pseudophosphorylation of single residues of the J-domain of DNAJA2 regulates the holding/folding balance of the Hsc70 system. *Protein Science*. 2024;33(8):e5105. <https://doi.org/10.1002/pro.5105>